The Effect of Amino Acids on the Fenton and photo-Fenton Reactions in Cloud Water: Unraveling the Dual Role of Glutamic Acid

Peng Cheng [1,2], *Gilles Mailhot* [1,3], *Mohamed Sarakha* [1], *Guillaume. Voyard* [1], *Daniele Scheres Firak* [4], *Thomas Schaefer* [4], *Hartmut Herrmann* [4], *Marcello Brigante* [1]*

[1] Université Clermont Auvergne, CNRS, Institut de Chimie de Clermont-Ferrand, F-63000 Clermont–Ferrand, France.

[2] Department of Environmental Engineering, School of Resources and Environmental Science, Wuhan University, 430079, PR China

[3] Université Clermont Auvergne, CNRS, Laboratoire de Météorologie Physique (LaMP), F-63000 Clermont–Ferrand, France.

[4] Atmospheric Chemistry Department (ACD), Leibniz- Institute for Tropospheric Research (TROPOS), 04318 Leipzig, Germany

*Corresponding author:

Marcello Brigante (Marcello.Brigante@uca.fr)

ABSTRACT

In this work, Glutamic acid (Glu) was selected as a model amino acid (AAs) to investigate its complexation with Fe(III) and Fe(II), focusing on its impact on the Fenton reaction and the photolysis of Fe(III) in cloud aqueous phase. Glu was found to enhance the rate constant for the reaction of Fe(II)-Glu with H_2O_2 to $1.54 \pm 0.13 \times 10^4$ M^{-1} s^{-1}, which is significantly higher than that of classic Fenton reactions (~50-70 M^{-1} s^{-1}). In contrast, the photolysis quantum yield of Fe(III)-Glu complex was determined to be 0.037 under solar simulated irradiation, largely lower than Fe(III)-hydroxy complexes (0.216). In the overall process (Fenton or Fe(III) photolysis), it was found that $^{\bullet}OH$ formation decreased in the presence of Glu. Additionally, the fate of Glu in the presence of Fe(III) was investigated as well as the oxidation process (driven by $^{\bullet}OH$ and ligand-to-metal charge transfer (LMCT) reaction) led to the formation of short-chain carboxylic acids and ammonium under simulated solar light. Interestingly, these two processes generated different primary short-chain carboxylic acids, indicating distinct mechanisms. This study provides valuable insights into the role and fate of amino acids in atmospheric chemistry, helping to further understand their impact on atmospheric processes.

KEYWORDS: Glutamic acid, Fenton, hydroxyl radical, oxidant capacity, atmospheric composition

SYNOPSIS

This study investigates the complexation of Fe(II) and Fe(III) with glutamic acid under cloud water conditions and the effect on Fenton and photo-Fenton reactions, hydroxyl radical formation, and their impact on amino acid oxidation.

1. INTRODUCTION

The Earth's atmosphere is a dynamic system in which different phases, including gases, aerosol particles, water droplets, and ice particles, are all engaged in complex chemical interactions that continually modify the atmospheric chemical composition (Bianco et al., 2020; Kanakidou et al., 2018). Among these, the cloud aqueous phase stands out as a critical reactive system, encompassing gaseous, liquid, and solid components. In recent years, intensified research efforts have centered on unraveling the composition of atmospheric cloud waters, significantly advancing our comprehension of multiphase chemistry within the atmosphere (Bianco et al., 2018). Common components identified in both aerosols and cloud water include inorganic ions, transition metal ions (TMI) such as iron (Angle et al., 2021; Bianco et al., 2017), and organic carbon (Battaglia Jr. et al., 2019), notably amino acids (AAs). However, the influence of AAs on iron redox chemistry and hydroxyl radical ($^{\bullet}OH$) production in cloud water remains insufficiently understood.

Recent investigations have unveiled the presence of reactive oxygen species (ROS) in viscous aerosol particles, highlighting their pronounced reactivity in such environments (Alpert et al., 2021; Edwards et al., 2022). Hydroxy radicals ($^{\bullet}OH$) emerge as primary ROS in the atmospheric water phase, with concentrations estimated between 10^{-14} to 10^{-12} M^{-1} (Bianco et al., 2020; Gligorovski et al., 2015). Key sources of $^{\bullet}OH$ include gas-droplet partitioning and in situ formation through processes like photolysis at surfaces or in the bulk phase, such as the photolysis of TMI and hydrogen peroxide (H_2O_2) (Bianco et al., 2015; Tilgner et al., 2013).

Iron (Fe), copper (Cu), and manganese (Mn) have gained prominence as pivotal metals in atmospheric chemical processes due to their elevated concentrations, with Fe averaging around 10^{-6} M in the atmospheric aqueous phase (Sorooshian et al., 2013). Experimental evidence and

literature emphasize the crucial role of iron, particularly via (photo)-Fenton and (photo)-Fenton-like processes, in the generation and budgeting of •OH (R1-R5) (Guo et al., 2014; Tilgner et al., 2013).

$$[Fe(H_2O)_6]^{3+} \xrightarrow{h\nu} [Fe(H_2O)_5]^{2+} + H^+ + {}^\bullet OH \quad \text{(R1)}$$

$$[Fe(H_2O)_5OH]^{2+} \xrightarrow{h\nu} [Fe(H_2O)_5]^{2+} + {}^\bullet OH \quad \text{(R2)}$$

$$[Fe(H_2O)_5]^{2+} + H_2O_2 \rightarrow [Fe(H_2O)_5OH]^{2+} + {}^\bullet OH \quad \text{(R3)}$$

$$[Fe(H_2O)_6]^{3+} + H_2O_2 \rightarrow [Fe(H_2O)_5]^{2+} + HO_2^\bullet + H_2O + H^+ \quad \text{(R4)}$$

$$[Fe(H_2O)_5OH]^{2+} + H_2O_2 \rightarrow [Fe(H_2O)_5]^{2+} + HO_2^\bullet + H_2O \quad \text{(R5)}$$

While Fe(III)/Fe(II) ions precipitate as oxides or hydroxides at pH higher than 4.0, in the cloud water phase, iron complexes with organic ligands enhance stability under typical cloud water photooxidation conditions (Soriano-Molina et al., 2018; Yuan et al., 2020). Various organic ligands, including carboxylic acids and aldehydes, have been extensively studied (Long et al., 2013; Marion et al., 2018; Soriano-Molina et al., 2018). However, less than 30 % of the dissolved organic carbon (DOC) in the cloud-aqueous phase has been molecularly characterized, with AAs constituting a significant portion of DOC (Bianco et al., 2016). Numerous field studies have confirmed the presence of AAs in cloud water, rain, fog, and aerosols, with concentrations typically ranging from low nanomolar to micromolar levels, depending on the location and sampling method (Matos et al., 2016; van Pinxteren et al., 2023; Renard et al., 2022; Triesch et al., 2021). For example, Renard et al. (2022) detected more than 15 AAs in cloud water collected at Puy de Dôme, France, with glutamate being one of the most abundant species. These compounds originate from both primary emissions (e.g., bioaerosols, ocean spray) and secondary atmospheric processes (e.g., processing of proteins or peptides within clouds) (Mace et al., 2003; Samy et al., 2011). Amino acids, as key nitrogen-containing

components in organic matter, can significantly affect the oxidation capacity of cloud water through free radical scavenging and metal complexation reactions (Bianco et al., 2016; Marion et al., 2018), but their specific atmospheric reactivity and transformation mechanisms are still unclear. The photochemical behavior and fate of AAs in the atmosphere remain relatively unexplored. For example, tryptophan can undergo direct photolysis, producing low-molecular-weight compounds and dimerization products under solar-simulated conditions. Recent investigations into the fate of the Fe(III)-aspartate complex demonstrate ligand-to-metal charge transfer reactions (LMCT) and the formation of ammonia and short-chain carboxylic acids (Marion et al., 2018).

However, the effect of the complexation between Fe(II) and AAs on the rate of Fenton reaction and the yield of $^{\bullet}$OH in the atmosphere has not yet been investigated. Moreover, the effect of the complexation between Fe(III) and AAs on the quantum yield of atmospheric photolysis of Fe(III) deserves further investigation, since both processes highly affect the budget of $^{\bullet}$OH during the day and night in the atmosphere. In addition, the complexation between Fe(III) and AAs introduces two distinct photooxidation pathways: the photolysis of Fe-AAs complexes and reactions between AAs and (photo)-generated $^{\bullet}$OH. Although both pathways significantly contribute to the transformation of AAs in cloud water and impact inorganic and organic chemical compositions, their mechanisms still lack further study, especially in terms of products generation.

This study specifically focuses on glutamic acid (Glu), an AA regularly detected in cloud water and aerosols (van Pinxteren et al., 2012; Triesch et al., 2021), and on the investigation of its impact on iron (Fe(II)/Fe(III)) reactivity. The study explored i) the effect of Glu on the rate and •OH yield of the Fenton reaction; and ii) the effect of Glu on the $^{\bullet}$OH production and Fe(II)

quantum yield during the Fe(III) photolysis. In addition, the study explores iii) two pathways of Fe(III) and Fe(III)-Glu complex photolysis: the LMCT process and the reaction between Glu and •OH, assessing their respective contributions to Glu fate. Utilizing competitive kinetic experiments, the contributions of each pathway were estimated, and a detailed investigation of the formation, and chemical mechanisms of transformation products was carried out. Ultimately, our study aims to quantify the diverse contributions of different pathways in amino acid conversion in the presence of iron.

2. MATERIAL AND METHODS

2.1. Chemicals

All chemicals were used without further purification: Fe(III)-perchlorate (99.9 %), Fe(II)-perchlorate (99.9 %), L-glutamic acid monosodium salt (Glu, 99 %), hydrogen peroxide (H_2O_2, 30 %), malonic acid (99.0 %), and 2,4-dinitrophenylhydrazine (DNPH, 97 %) were purchase from Sigma Aldrich. Sodium formate (99.0 %), potassium oxalate monohydrate (99.0 %), sodium succinate dibasic (98.0 %), and 3-(2-pyridyl)-5,6-diphenyl-1,2,4-triazine-p, p'-sulfonic acid monosodium salt hydrate (Ferrozine, 97 %) were purchased from Fluka. Ammonium acetate (99.3 %) was purchased from Fisher. Water was purified using a reverse osmosis RIOS 5 and Synergy (Millipore) device (resistivity 18.2 MΩ cm, DOC < 0.1 mg L^{-1}). All solutions were prepared in milli-Q water.

2.2. Experimental procedure

2.2.1. Fenton reaction

The Fenton experiments were carried out with Fe(II) perchlorate at room temperature and a pH of 5.6 ± 0.1 (Kinetic experiments) and 3.8 ± 0.1 (Electron spin resonance (ESR) experiments).

The pH of 5.6 was chosen to favor the formation of Fe(II)-Glu complexes during the kinetic studies, while the lower pH of 3.8 was selected for ESR experiments, as •OH detection by ESR is more effective under acidic conditions. These two pH values fall within the typical range observed in atmospheric cloud water. Specifically, pH of 3.8 represents more acidic conditions often found in polluted regions, whereas pH of 5.6 reflects the composition of cloud water in remote or less impacted environments (Pye et al., 2020; Shah et al., 2020). This range enables the assessment of the system's behavior under environmentally relevant conditions.

The Fenton kinetic experiments were initiated by the addition of the H_2O_2 stock solution. Hence, the designed H_2O_2 concentration are 100 and 25 μM in kinetics and ESR experiment respectively. The solution was continuously stirred during the reaction. The pH of the solution was adjusted using $HClO_4$ or NaOH solutions. The samples were taken every 15 seconds and mixed with a solution of Ferrozine in phosphate buffer (pH = 7.0 ± 0.1) (Gabet et al., 2023). Phenol was used as •OH scavenger in the experiment. As a scavenger, the required concentration of phenol was calculated to quench •OH so that theoretically 99 % of •OH can be trapped via reacting with phenol. The same method was used in the presence of Glutamic acid (Glu) to study the Fe(II)-Glu complex Fenton-like reaction at the same pH. To get different fractions of Fe(II)-Glu, Fe(II) was mixed with varying concentrations of Glu solution (0 - 25 mM) to calculate the rate constant of the Fenton reaction. The experimental data were analyzed using Origin 2019 software. To determine and quantify the •OH generation in the Fenton reaction, the ESR experiment was carried out using 5,5-dimethyl-1-pyrroline-N-oxide (DMPO) as the spin trap. $Fe(ClO_4)_2$ and H_2O_2 were mixed with DMPO at a pH of 3.8 ± 0.1. The pH was set because the ESR signal intensity was lower at a higher pH = 4.0. ESR spectroscopy was

155 performed on a Bruker EMX-plus spectrometer using the resonator 4119HS. Detailed
156 information was provided in the supplementary material section (**SM1**).

157 **2.2.2. Photolysis of Fe(III)**

158 To study the Fe(III) photolysis, isopropanol was used as a scavenger in the solution to quench
159 the generated •OH radicals. The pH of the solution was adjusted to 3.8 ± 0.1 with $HClO_4$ or
160 NaOH solutions. The Fe(III) solution was irradiated in a Pyrex jacked cylindrical reactor (**Fig.**
161 **SM1**) with a circulation cooling system to keep a constant temperature of 283 ± 0.2 K. The
162 reactor was located at the focal point of a 500 W xenon lamp equipped with a Pyrex filter to
163 remove wavelengths < 290 nm and a water filter for infrared radiation absorption. The solution
164 was stirred with a Teflon-coated magnetic stirring bar to ensure homogeneity. The same setup
165 was used for the photolysis experiments in the presence of Fe(III)-Glu complexes. Different
166 fractions of Fe(III)-Glu were achieved by adding different amounts of a Glu 50 mM stock
167 solution (designed [Glu] = 0 - 200 μM).
168 The emission spectrum of the irradiation setup was recorded using a calibrated CCD camera
169 (Ocean Optics USB 2000+UV-Vis) coupled with an optical fiber. An irradiance of 8.38×10^3
170 μW cm^{-2} was determined between 290 and 500 nm as shown in **Fig. SM2**. Compared to the
171 natural solar emission spectrum, the UV region between 290 and 400 nm, which contribute for
172 driving the photoreaction of Fe(III) and Fe(III)-Glu, shows a quite similar spectral profile, as
173 reported in our previous publication (Bianco et al., 2015). The Energy and photonic flux (I_0) of
174 the polychromatic irradiation at every nanometer wavelength are listed in **Table SM1**. Detailed
175 information about the calculation of the Fe(III) and Fe(III)-Glu photolysis quantum yield is
176 given in the supplementary material section (**SM2**). To quantify the •OH generation during the
177 Fe(III) photolysis, isopropanol was used in excess (10 mM) as a selective •OH probe.

Isopropanol reacts with •OH to form acetone which was quantified by HPLC (see section 2.4) (Motohashi and Saito, 1993).

2.2.3. Photodegradation of Glu

To investigate the fate of Glu in various systems, experiments were performed using the previously described photoreactor setup. Glu solutions, either alone or mixed with Fe(III) and/or H_2O_2, were irradiated under simulated solar light at pH 3.8 ± 0.1. Samples were collected at specific time intervals and analyzed using HPLC-MS (see section 2.4). To calculate and compare the photodegradation kinetics of Glu in different systems, a pseudo-first-order kinetic model was applied, expressed as Equation (1):

$$-\ln(C_t/C_0) = k_{obs}\, t \qquad \text{Eq (1)}$$

where C_0 represents the initial concentration of Glu, and C_t is the concentration of Glu at time t of irradiation. In addition, IC-MS and TOC analyses were performed to identify the generated by-products and assess the mineralization of Glu (see section 2.4).

2.3. Study of the speciation of the Fe(III)/Fe(II)-Glu complex

The speciation of the Fe(III)/Fe(II)-Glu complex was studied using the Hyss 2009 software. This analysis included the iron, iron-aqua, iron hydroxy, and iron-Glu complexes in the solution. The parameters used in the software, such as iron and Glu concentrations, kept consistent with the one in the experimental procedure. The stability constants (log K) used for the complexes, such as the Fe(II)-Glu and Fe(III)-Glu complexes, etc. are listed in **Table SM2**. These constants are derived from the Visual MINTEQ database or NIST database 46 and have been corrected for a temperature of 25 °C and an ionic strength (I) of 0 M. The detailed method is provided in the supplementary material section (**SM3**).

2.4. Chemical analysis

2.4.1. Fe(II), H_2O_2, and Acetone quantification

Iron (II) concentration was determined by using Ferrozine, which forms a stable magenta complex with Fe(II) (Fe(II)-ferrozine) (Gabet et al., 2023). Hydrogen peroxide concentration during experiments was determined by using a spectrofluorimetric quantification method (Bader et al., 1988). The concentration of generated acetone in the solution was evaluated by HPLC (Shimadzu NEXERA XR HPL) equipped with a photodiode array detector and an autosampler (Wang et al., 2005). **Fig. SM3** shows the calibration curve of Fe(II), H_2O_2, and acetone. More details are given in the supplementary material section (**SM4**).

2.4.2. UPLC-MS, IC-MS and TOC

The quantification of Glutamic acid (Glu) and the identification of its transformation products was conducted using a ThermoScientific Orbitrap Q-Exactive high-resolution mass spectrometry (HRMS) coupled with a ThermoScientific Ultimate 3000 RSLC ultra-high-performance liquid chromatography (UPLC) system. The quantification of carboxylic acid by-products and NH_4^+ resulting from Glu degradation was performed using a Thermo-Fisher Scientific ICS-6000 Ionic chromatograph interfaced with a simple quadrupole mass spectrometer (ISQ-EC-Thermo Scientific). The total organic carbon (TOC) concentration in the aqueous solution was followed by a Shimadzu TOC 5050A analyzer. Detailed information is reported in the Supplementary Material section (**SM5**).

2.5. Kinetic Modeling

To verify the obtained experimental rate constants of the reaction between Fe(II)-Glu and H_2O_2, COPASI software was utilized to simulate the kinetics of Fe(II) consumption and generation of

222 •OH in the Fenton reaction in the presence of Glu using the default settings of the deterministic
223 LSODA algorithm to solve ordinary differential equations (Hoops et al., 2006). The chemical
224 reactions considered in the model are provided in **Table SM3**. The majority of rate constants
225 used in the model were available in the literature or obtained from experimental results. For the
226 unknown or uncertain rate constants, the value is obtained from the estimation according to a
227 similar reaction.

228 **3. RESULTS AND DISCUSSION**

229 To investigate the effect of Glu on the Fe(II)/Fe(III) cycle, a complex set of experiments was
230 performed. First, the complexation of Fe(II)/Fe(III) with Glu was studied as a function of pH
231 and the initial concentration of Glu. Second, to study the effect of Glu on the Fenton reaction,
232 its rate constants and •OH generation in the presence of Glu were obtained experimentally and
233 using the kinetic model. The formation rates of Fe(II) and •OH were determined from Fe(III)
234 photolysis with or without Glu. Finally, the mechanism of Glu photo-transformation was
235 reported.

236 **3.1. Complexation of Glu with Fe(II)/Fe(III)**

237 The Fe speciation was initially investigated to understand how Glu interacts with iron ions
238 under various conditions with Hyss2009 software. **Fig. SM4a** shows the speciation of 20 μM
239 Fe(II) in the presence of Glu (0.2 – 25 mM) across a pH range of 4 to 10. It can be observed
240 that Fe(II) predominates until pH = 5, while the fraction of the Fe(II)-Glu complex increases
241 after this pH. Hence, a higher pH (5.6) was selected for the Fenton reaction to guarantee the
242 presence of complex, while still working under aerosol/cloud conditions and to avoid iron
243 precipitation occurring at higher pH values. At pH 5.6, the Fe(II)-Glu complex accounts for

244 2.2 % in the presence of 20 µM Fe(II) and 25 mM Glu. The complex fractions at varying Glu
245 concentrations at pH = 5.6 are provided in **Table SM4**.
246 **Fig. SM4b** shows the simulated speciation of Fe(III) (100 µM) as a function of pH in the
247 presence of Glu (10-20 µM). The Fe(III)-aqua, Fe(III)-hydroxy complexes, and Fe(III)-Glu
248 complexes were observed as a function of the pH. At pH = 3.8, [Fe(III)] = [Glu] = 100 µM, the
249 Fe(III)-hydroxy complexes $Fe(OH)^{2+}$ and $Fe(OH)_2^{+}$ represent 24.4 and 22.8 % of the total Fe(III)
250 concentration, respectively. In contrast, Fe(III)-Glu complex accounts for 52.3 % of the total
251 Fe(III), while Fe(III)-aqua complex constitutes only 0.5 %. The UV-Vis spectra of Fe(III), Glu,
252 and Fe(III)-Glu complex are depicted in **Fig. SM2**. The characteristic absorption band of Fe(III)
253 with a maximum at 297 nm, corresponding to the charge transfer bands of $Fe(OH)^{2+}$, becomes
254 attenuated in the presence of Glu. Moreover, the UV-Vis spectrum of Fe(III)-Glu mixture
255 differs from those of Fe(III) and Glu alone or the simple overlap of their individual spectra,
256 confirming the formation of a stable Fe(III)-Glu complex (Samavat et al., 2007). The fractions
257 of the generated complex in the presence of different Glu concentrations at pH = 3.8 are given
258 in **Table SM5**. For the sake of simplicity, Fe(III)/Fe(II)-hydroxy and Fe(III)/Fe(II)-aqua
259 complexes are hereafter referred as Fe(III) and Fe(II).

260 **3.2. Fenton reaction process in the presence of Glu**

261 **3.2.1. Fe(II) oxidation**

262 To study the effect of Glu on the kinetics of the Fenton reaction and determine the rate constant
263 of the reaction of Fe(II)-Glu with H_2O_2, experiments were performed using different
264 concentrations of Glu. **Fig. 1a** shows the faster Fe(II) concentration decreases when the Glu
265 concentration increases, which indicates that Glu can increase the reaction rate of Fe(II) with
266 H_2O_2. This is likely due to the formation of the Fe(II)-Glu complex which has a high reaction

rate constant with H_2O_2. As seen in **Fig. 1b**, the data obtained by plotting $\frac{-\frac{d[Fe(II)]}{dt}}{[H_2O_2][Fe(II)]}$ as a function of the fraction of Fe(II)-Glu can be fitted with a linear equation y = ax + b, where a is equal to 1.54 ± 0.13×10^4 M^{-1} s^{-1} and represents the rate constant of reaction of Fe(II)-Glu with H_2O_2 , and b is equal to rate constant of Fe(II) with H_2O_2 ($-\frac{d[Fe(II)]}{dt}$ data is provided in **Table. SM4**). Notably, obtained rate constant is much higher than the rate constant of the classic Fenton reaction which has a rate constant of about 50-70 M^{-1} s^{-1} (Kremer, 2003; Neyens and Baeyens, 2003; Rachmilovich-Calis et al., 2009). Moreover, the value is about five times higher than our recently reported value for the reaction between Fe(II)-oxalate and H_2O_2 (3.2 ± 0.3 × 10^3 M^{-1} s^{-1}) (Scheres Firak et al., 2025). Despite the quantitative difference, both two obtained values are of the same order, highlighting the significant reactivity enhancement conferred by organic ligand coordination. The reason behind this increase is likely due to the Fe(II)-Glu complex accessing a lower reduction potential calculated to be + 0.241 V compared with the Fe(II) (+ 0.771 V) (Strathmann and Stone, 2002), which contributes to the higher rate constant of the reaction of Fe(II)-Glu with H_2O_2.

Then the Fenton reaction model was used to fit the experimental data to verify the rate constant value of the reaction between Fe(II)-Glu and H_2O_2. As shown in **Fig. 1a**, the experimental data of Fe(II) kinetics can be well-fitted by the model. The fitted rate constant value of the reaction between Fe(II)-Glu and H_2O_2 was obtained at a range of 1.2×10^4 to 1.8×10^4 M^{-1} s^{-1}, which is very close to the experimental results.

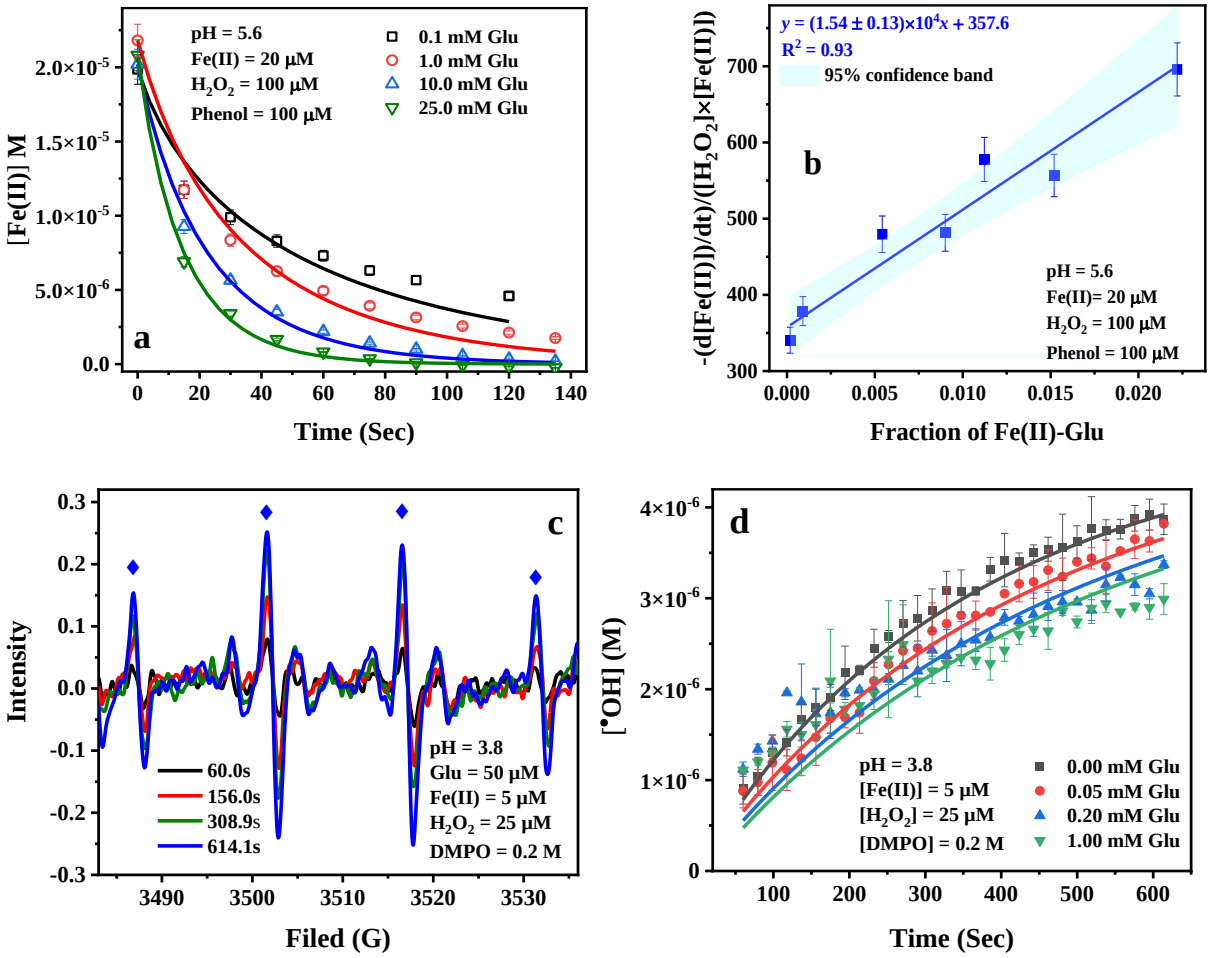

Fig. 1 *Effect of different concentrations of Glu on the kinetics of Fenton reaction (a), apparent rate constant as a function of the fraction of Fe(II)-Glu (b), Signal of EPR corresponding to DMPO-OH (The symbol "◆" marks the position of the characteristic 1:2:2:1 EPR signal of the DMPO-OH adduct.) (c), the kinetics of •OH generation in Fenton reaction in the presence of different concentrations of Glu, (d). Points are determined experimentally, and lines in figures* ***a*** *and* ***d*** *are the fit of data using the kinetic model.*

3.2.2. •OH quantification

To study the effect of Glu on the •OH generation, EPR experiments were carried out. **Fig. 1c** shows the EPR signal of DMPO-OH (1:2:2:1) increases with the reaction time, indicating that

297 •OH is continuously generated. In **Fig. 1d**, the concentration of generated •OH decreases when
298 the Glu concentration increases from 0 to 1.0 mM. This trend suggests no direct •OH generation
299 occurs from the reaction of Fe(II)-Glu with H_2O_2. This hypothesis has been verified by
300 employing a kinetic model. The experimental data can be well fitted using the experimental rate
301 constant $k_{Fe(II)\text{-}Glu/H_2O_2} = 1.54 \pm 0.13\times10^4$ M^{-1} s^{-1}.

302 **3.3. Fe(III) photolysis in the presence of Glu**

303 **3.3.1. Fe(II) formation**

304 To study the effect of Glu on the kinetics and determine the quantum yield of the photolysis of
305 Fe(III), the photo-driven reaction was carried out in the presence of different concentrations of
306 Glu (0-200 μM) under simulated solar light. **Fig. SM5a** shows that the Fe(II) generation rate
307 decreases when the Glu concentration increases, which indicates that Glu slightly reduces the
308 photoactivity of Fe(III). As shown in **Fig. 2a**, plotting the apparent quantum yield of Fe(II),
309 $\Phi_{Fe(II)}^{obs}$, as a function of the fraction of Fe(III)-Glu complex, the quantum yield of Fe(II)
310 decreases with the fraction of Fe(III)-Glu complex increasing. The linear fit can depict the
311 kinetic data well with a regression coefficient equal to 0.99. As mentioned in **SM2**, the intercept
312 represents the Fe(II) quantum yield of Fe(III) photolysis under polychromatic irradiation, which
313 is equal to 0.216 ± 0.004. This result is consistent with previous data (Bossmann et al., 1998).
314 The slope represents the difference between Fe(II) quantum yield of the Fe(III) photolysis and
315 the value of the photolysis of Fe(III)-Glu complex ($\Phi_{Fe(III)-Glu}^{Fe(II)} - \Phi_{Fe(III)}^{Fe(II)}$), which is equal to -
316 0.179, hence the Fe(II) quantum yield during the photolysis of Fe(III)-Glu is calculated to be
317 0.037 ± 0.004. Weller et al.(Weller et al., 2013) investigated the photolysis of Fe(III)-
318 carboxylate complexes and found the quantum yield of Fe(II) formation from Fe(III)-malonate

at 308 nm and 351 nm, with values of 0.024 ± 0.001 and 0.040 ± 0.003 respectively. This suggests that Fe(III) complexes containing unsubstituted carboxylates as a functional group exhibit lower quantum yields compared to Fe(III).

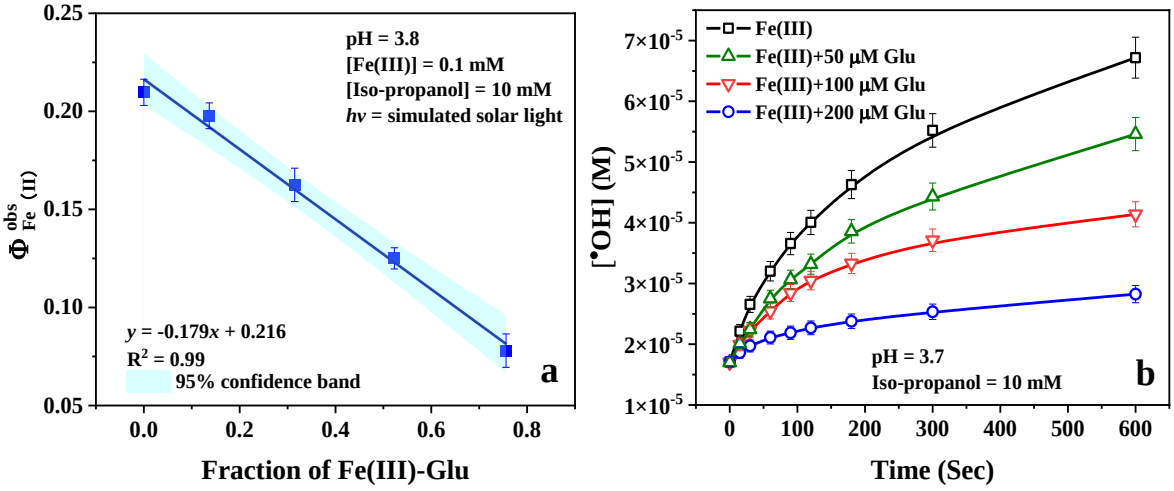

Fig. 2 *a) The quantum yield of Fe(III) photolysis as a function of the fraction of Fe(III)-Glu complex; b) The •OH generation of Fe(III) photolysis in the presence of different concentrations of Glu. The continuous lines are visual guides generated by applying the "Connect B-Spline" function in Origin 2019.*

3.3.2. •OH generation

Since the photolysis of Fe(III) is an important process affecting the budget of •OH in the atmosphere (Guo et al., 2014), the effect of Glu on the •OH produced by the photolysis process of Fe(III) was investigated. As shown in **Fig. SM5b,** the acetone generation rate decreases when the Glu concentration increases, indicating that the •OH generation of the Fe(III) photolysis decreases in the presence of Glu (**Fig. 2b**). The most likely reason for this observation is the decrease of the Fe(III) hydroxy complexes (**Table SM5**), hence the decrease of the •OH yield as the Fe(III)-Glu does not produce •OH directly, but instead forms Glu oxidation products

335 (Glu_{ox}) through the LMCT process. These Glu oxidation products can complex Fe(II) and
336 regenerate Fe(III), a mechanism known as "the quenching mechanism" proposed by Wang et
337 al (2010)(Wang et al., 2010). This process reduces the apparent quantum yield of Fe(II) to 0.037
338 ± 0.004. This result illustrates that •OH generation could be less in the presence of amino acids
339 during the daytime in the atmosphere.

340 **3.4. The Glu fate in the presence of Fe(III) under simulated solar light**

341 **3.4.1 Photodegradation of Glutamic acid in different systems**

342 All the above results indicate that Glu not only stabilizes Fe(III)/Fe(II) at higher pH but also
343 influences the Fenton reaction and photolysis of Fe(III) processes. The main effects were that
344 the complexes altered the individual reaction rate constants and •OH production. On the other
345 hand, Glu as the organic ligand can also be degraded during the reaction, especially photo-
346 reaction in the atmosphere. **Fig. 3** shows the photodegradation kinetics of Glu in different
347 systems, and the first-order fitted data is reported in **Fig. SM6**. As expected, when only Glu
348 was present in the solution, no significant degradation ($k_{obs} = 1.90 \pm 0.22\times10^{-5}$ s^{-1}) was observed
349 after 1 hour of irradiation, as shown in the UV-Vis spectrum (**Fig. SM2**) of Glu, since there is
350 no significant light absorption in the solar spectrum. The Glu degradation slightly increased in
351 the presence of 1 mM H_2O_2 with a degradation constant of $2.44 \pm 0.45\times10^{-5}$ s^{-1} corresponding
352 with a degradation of 8.5 % in 1 hour, which is due to the formation of •OH radicals via the
353 photolysis of H_2O_2. In addition, the rate constant of •OH with Glu is 2.3×10^{8} M^{-1} s^{-1} (Masuda
354 et al., 1973), which means that the reaction between those two components is one of the most
355 important processes for the degradation of Glu. Considering the second reaction rate constant
356 between •OH and H_2O_2 ($k_{H_2O_2}^{\bullet OH} = 2.7\times10^{7}$ M^{-1} s^{-1}) (Christensen et al., 1982), it can be argued

that under adopted conditions, about 55 % of generated •OH was quenched by the H_2O_2, which led to the formation of less reactive hydroperoxyl radical/superoxide anion pair ($HO_2^{\bullet}/O_2^{\bullet-}$).

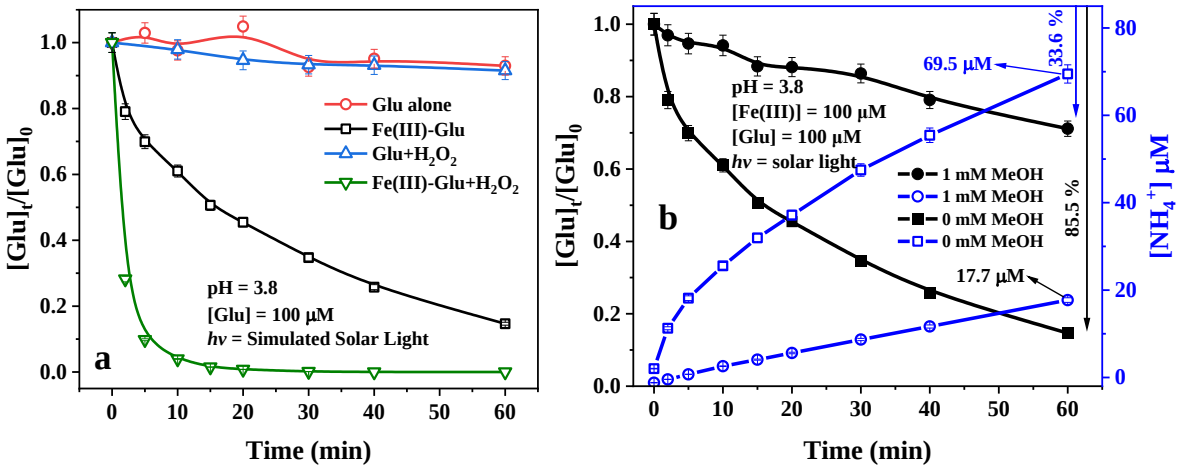

Fig. 3 *a) Photodegradation of Glu in different systems: Glu alone, Fe(III)-Glu; Glu+H_2O_2 and Fe(III)-Glu+H_2O_2 ([Glu] = 100 µM, [Fe(III)] = 100 µM, [H_2O_2] = 1 mM). b) Photodegradation of Glu and ammonium generation in the Fe(III)-Glu system in the absence and presence of MeOH. The continuous lines are visual guides generated by applying the "Connect B-Spline" function in Origin 2019.*

Moreover, in the presence of Fe(III), the mixture of Fe(III)-hydroxy and Fe(III)-Glu complexes underwent the photolysis process. As shown in **Fig. 3a**, about 85 % of Glu was degraded with a first-order rate constant of $4.99 \pm 0.24 \times 10^{-4}$ s^{-1} after 1 hour of irradiation. This high efficiency is likely due to two different Glu degradation pathways, one is due to the reaction between Glu and the •OH radicals generated by photolysis of Fe(III) (R1 and R2), and the other one is due to the direct photolysis of Fe(III)-Glu leading to the formation of Fe(II) and oxidation products of the organic ligand (Glu_{ox}). The synergistic effect of those two processes highly improved the Glu degradation efficiency. To distinguish between the contributions of the two degradation pathways, methanol was selected as •OH scavenger ($k^{\bullet OH}_{Methanol} = 9.7 \times 10^8$ M^{-1} s^{-1}) (Buxton et al.,

1988). As illustrated in **Fig. 3b**, Glu degradation was inhibited by 60 %, indicating that 40 % of Glu degradation originates from the photolysis of Fe(III)-Glu complexes. Interestingly, this ratio aligns with the proportion of Fe(III) and Fe(III)-Glu complexes in the system (**Table SM5**), confirming the aforementioned conclusion. Furthermore, the degradation of Glu resulting from the photolysis of Fe(III)-Glu complexes likely does not involve a $^{\bullet}OH$ process (Sun et al., 1998; Weller et al., 2013).

Glu degradation was observed to be approximately 100 % after 20 mins of irradiation in the presence of Fe(III) and H_2O_2, with a first-order rate constant of $5.13 \pm 1.03 \times 10^{-3}$ s^{-1}. Compared to conditions with only Fe(III) or H_2O_2, the efficiency of Glu degradation significantly improves due to the photo-Fenton reaction in the system, which greatly accelerates the formation rate of reactive species and consequently enhances the degradation rate of Glu.

3.4.2. Analysis of photodegradation products of glutamic acid

To distinguish the Glu degradation processes resulting from the photolysis of Fe(III)-Glu complexes and from those caused by $^{\bullet}OH$ attack, which might lead to the formation of different products, a series of experiments were conducted. In all cases, IC-MS was employed to analyze the formation of short-chain carboxylic acid and ammonium ions, providing a deeper understanding of the photochemical reaction products in various systems under simulated solar light.

Figure 4a depicts the formation of ammonium (NH_4^+) in different systems under irradiation. A positive correlation is observed between the rate of NH_4^+ production and the rate of Glu degradation in various systems, suggesting the occurrence of deamination during the Glu degradation. Additionally, several carboxylic acids (i.e. acetic, formic, succinic, malonic, and

oxalic acids) were detected (**Table SM6**), as illustrated in **Fig. 4b**, **4c**, and **4d**. Notably, the concentration of generated carboxyl acids is considerably lower than that of NH_4^+.

After 120 min of irradiation, low concentrations of generated NH_4^+ and carboxylic acid were determined during Glu photolysis due to small Glu degradation (see **Fig. 4a** and **Fig. SM7**). In the presence of 1 mM H_2O_2, NH_4^+ concentration increased to 7.8 μM within 120 min, representing a 3-fold increase compared to that produced during Glu photolysis. **Fig. 4b** demonstrates the formation of carboxylic acids with formate and succinate as primary carboxylate products, while a negligible concentration of acetate (less than 1 μM) was also detected, all of which are products of •OH attack.

In the presence of Fe(III), NH_4^+ concentration increased to 69.5 μM (**Fig. 4a**) within 60 min. Simultaneously, the generation of carboxyl acids, such as formate, acetate, and oxalate was observed. The concentration of formate initially increased, reaching a maximum value of 8.7 μM at 20 min, followed by a decline to about 6.4 μM at 60 min. The reason for the decline is probably due to the reaction of formate with photo-generated •OH ($k_{\text{Formate}}^{\bullet\text{OH}} = 1.3{-}1.4 \times 10^8\ \text{M}^{-1}\ \text{s}^{-1}$) (Buxton et al., 1988). Acetate concentration steadily increased throughout the reaction, reaching 10.9 μM at 60 min. Other carboxylates, such as succinate, malonate, and oxalate, were found in lower concentration, with a maximum of around 2 μM within 5 min. As mentioned above, in the presence of Fe(III), the Glu degradation can be attributed to two pathways: one resulting from •OH attack, on the other from the photolysis of the Fe(III)-Glu complexes.

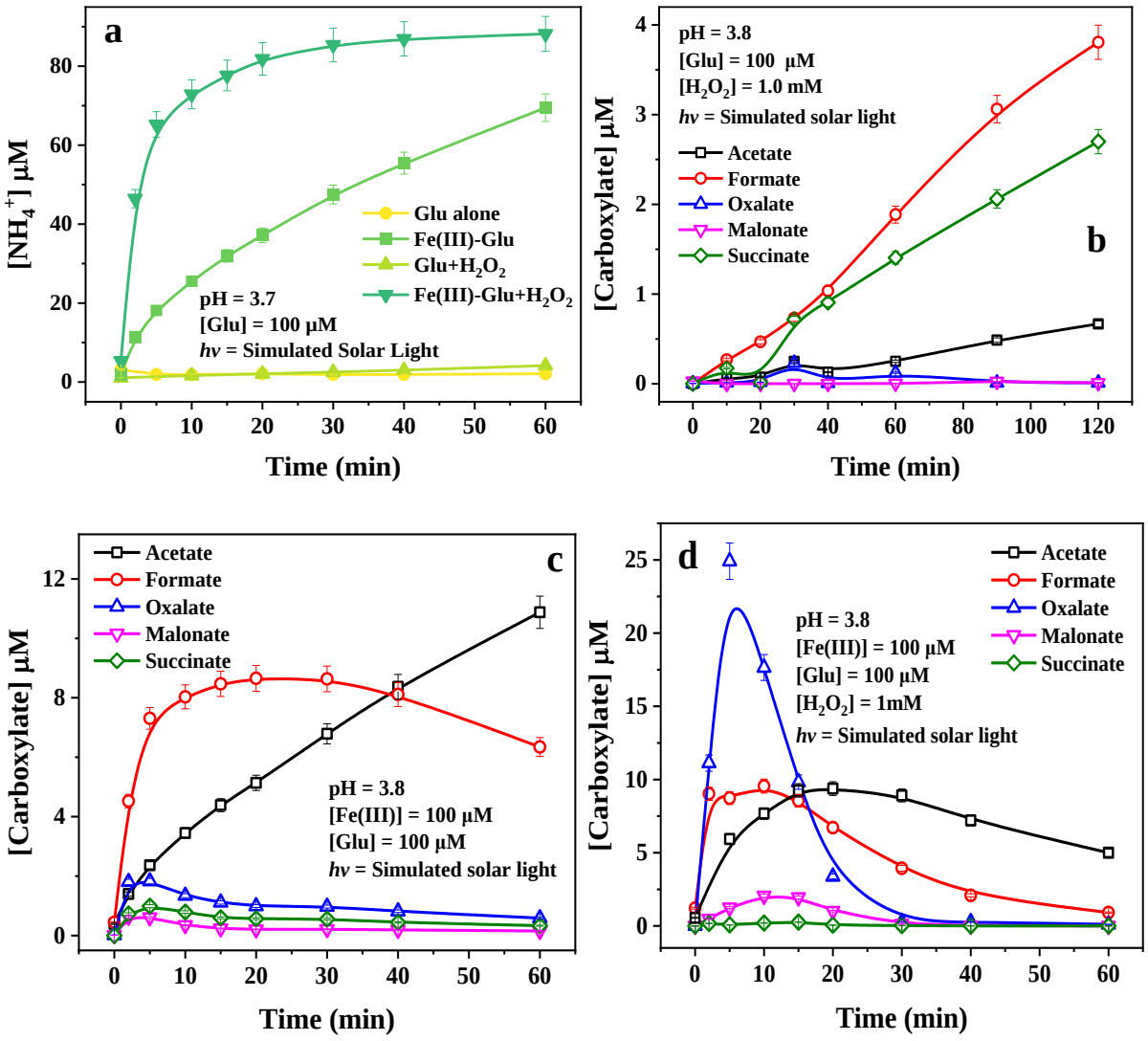

Fig. 4*. The by-products of Glu degradation under solar light a) formation of NH_4^+ in different systems; formation of carboxylic acids b) in the system Glu+H_2O_2; c) in the system Glu+Fe(III) and d) in the system Glu+Fe(III)+H_2O_2. The continuous lines are visual guides generated by applying the "Connect B-Spline" function in Origin 2019.*

To distinguish the contribution of these two pathways, isopropanol was employed to quench •OH in solution generating acetone as the main product (Motohashi and Saito, 1993). As shown in **Fig. SM8**, only acetate and formate were generated (succinate, malonate, and oxalate were not detected). Moreover, the presence of isopropanol significantly enhanced the formation of

acetate compared to values observed with only Fe(III) and Glu. This is likely due to the H-donor effect of the added alcohol or to the reaction between acetic acid radicals ($HOOCCH_2^{\bullet}$) and $HO_2^{\bullet}$ radicals, the latter being generated through the reaction of $^{\bullet}OH$ with the alcohol. As shown in **Fig. SM8**, the concentration of generated formate in the presence of isopropanol and Fe(III) is lower than that when only Fe(III) is added, suggesting that formate was likely not a primary product generated from the photolysis of Fe(III)-Glu complexes but rather may be produced by $^{\bullet}OH$ attack of other carboxylic acids. For example, the generated acetate can be further oxidized reacting with $^{\bullet}OH$ leading to the formation of formate.

This finding is consistent with the result observed in the presence of H_2O_2 alone (**Fig. SM7**). In the presence of $^{\bullet}OH$ scavenger, the generation of NH_4^+ was strongly inhibited with the formation of 17.7 μM instead of 69.5 μM after 1 h (as previously reported in **Fig. 3b**), which indicates that the NH_4^+ formation is mainly due to the $^{\bullet}OH$ attack process. Furthermore, a significant NH_4^+ (up to 69.5 μM within 60 min) can be observed in the presence of both Fe(III) and H_2O_2 (**Fig.4d**). Oxalate, acetate, and formate were observed as the predominant carboxylate products with higher concentrations, reaching 24.9, 9.4, and 9.6 μM respectively, before decreasing. Additionally, the formations of malonate (2.1 μM) and succinate (0.3 μM) were observed at lower concentrations during the photoreaction. In the presence of H_2O_2 and Fe(III), the Fe(III)/Fe(II)-cycle is enhanced via the photo-Fenton reaction. Fe(II) is rapidly re-oxidized to Fe(III) to produce $^{\bullet}OH$, which then directly attacks Glu, leading to degradation. Fe(III) is re-complexed by Glu reactivating the photoreaction and then the iron cycle. Therefore, the addition of H_2O_2 favors deamination as well as various carbon-centered radical combination interactions. The rapid depletion of oxalate after 30 min implies that photolysis of complexes between Fe(III) and polycarboxylic acid also occurs in this system, while formate, acetate, and

malonate exhibit similar tendencies with different reaction rates. To verify the mineralization of Glu during the reaction, a TOC was followed during the reaction. As shown in **Fig. SM9a**, the mineralization efficiency of Glu in the presence of Fe(III) and H_2O_2 is significantly higher than that observed when only Fe(III) is present, due to the presence of the photo-Fenton process. This finding is consistent with the degradation efficiency of Glu presented in **Figure 3a**. Hence, these results illustrate that Glu was mineralized to form CO_2 and H_2O. Moreover, the TOC values obtained experimentally are higher than the values calculated from the concentration of Glu and carboxylic acid products, indicating the presence of other organic compounds in the system. Along these organic substances cannot be detected under our experimental conditions, they will enter the cloud water gas phase, further participating in atmospheric photochemical reactions and eventually being mineralized into H_2O and CO_2. In the presence of H_2O_2, as Glu undergoes photodegradation, the concentration of H_2O_2 in the system continues to decrease until it is completely consumed (**Fig. SM9b**).

3.5. Insight into the mechanism of Glu transformation

The light-driven transformation mechanism of Glu in the presence of Fe(III) was investigated, with a focus on the $^{\bullet}OH$-mediated and the ligand-to-metal charge transfer (LMCT) process. The key difference between the two processes lies in the generation of glutamate radials: the $^{\bullet}OH$-mediated process involves a free radical mechanism initiated by hydrogen abstraction, whereas the LMCT pathway proceeds via an electron transfer process driven by photoexcitation. To provide a clear comparison, the two mechanisms are illustrated separately in **Scheme. 1** summarizing the possible Glu degradation pathway, derived from IC-MS analysis of the detected products.

In the •OH-mediated process, the α- carbon of Glu is identified as the primary site attacked for •OH attack, initiating the transformation process. Hydrogen abstraction by •OH results in the formation of glutamate alkyl radical (R-C•(COO^-)NH_3^+) and H_2O. Subsequently, this alkyl radical reacts with O_2 to generate the alkylperoxy radical (ROO•), which is further converted to alkoxy radical (RO•) (Goldman et al., 2021; von Sonntag and Schuchmann, 1991). The formation of RO• is followed by a deamination process, which leads to the formation of ammonium (NH_4^+) and 2-oxoadipic acid through the cleavage of the amino group (Vel Leitner et al., 2002). Due to the presence of an oxo group (C=O) adjacent to a carboxyl group (COOH), 2-oxoadipic acid is chemically unstable and prone to self-decomposition via decarboxylation, resulting in the formation of succinic acid (Penteado et al., 2019). Further oxidation of succinic acid produces smaller carboxylic acids (Charbouillot et al., 2012).

In contrast, the LMCT process is initiated upon irradiation, resulting in the reduction of Fe(III) to Fe(II) and the generation of a radical centered on the oxygen atom of α-carboxyl group of glutamic acid (R-CH(NH_3^+)$C^+O•O^-$). This high reactive radical undergoes a decarboxylation process resulting in the formation of an alkyl radical (R-CH•NH_3^+). Subsequently, the radical chain reaction propagates in the presence of O_2, leading to the formation of smaller carboxylic acids. It is critical to highlight that the only carboxylic acids detected under the same conditions are formic acid and acetic acid. This is different from the •OH-mediated process, in which succinate is first formed and then further decomposed into compounds such as other small molecular carboxylic acids.

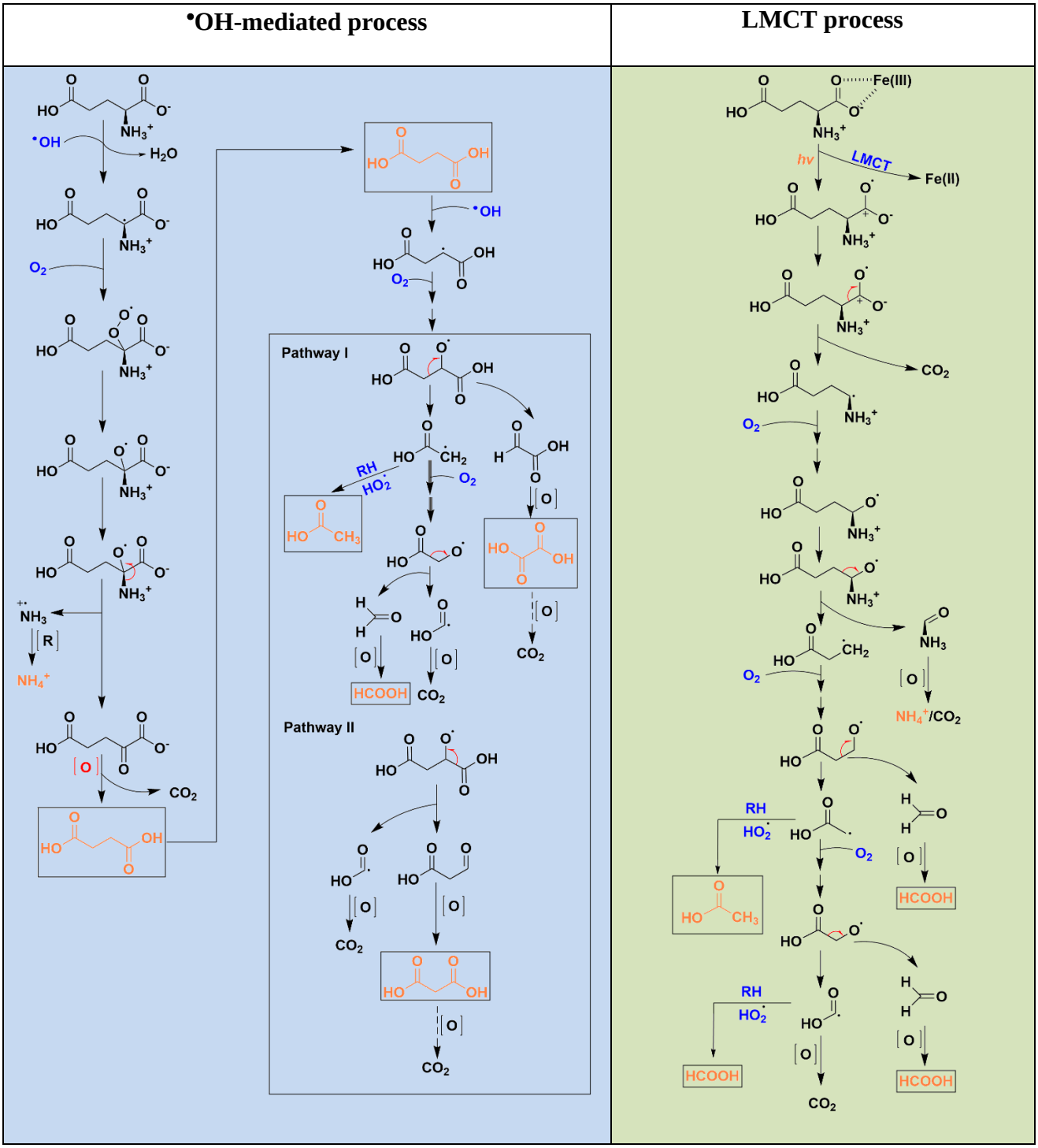

492 ***Scheme 1.*** *The mechanism of Glu degradation in the presence of Fe(III): by •OH attacking*

493 *process and LMCT process. Products in orange are detected by IC-MS.*

494

4. ATMOSPHERIC IMPLICATION

This study systematically investigated the complexation of Glu with Fe(II)/Fe(III), its effect on the typical atmospheric reactions (Fenton reaction and Fe(III) photolysis), and its fate in the atmospheric aqueous phase. Our findings reveal that iron-amino acid complexes (Fe-AAs) significantly modify the Fe(II)/Fe(III) cycle and •OH budget, diverging from the "classic" photo-Fenton mechanisms. Specifically, Fe(II)-Glu reacts with H_2O_2 at a rate constant two orders of magnitude higher than Fe(II) alone, potentially improving the iron cycle. Conversely, Fe(III)-Glu exhibits a lower quantum yield under irradiation, suppressing the Fe(III)/Fe(II) cycle. Moreover, both reactions result in lower •OH generation, as they favor the formation of Glu oxidation products (Glu_{ox}), thus partially affecting atmospheric oxidative capacity.

To date, the concentration of the Fe(II)/Fe(III)-Glu in cloud water has not yet been directly measured. Hence, based on the reported mean concentrations of Glu (87 nM) (Renard et al., 2022), Fe(II) (1 μM) (Deguillaume et al., 2014), and Fe(III) (0.5 μM) (Deguillaume et al., 2014) in cloud water from the Puy de Dôme station (PUY - France), the fraction of Fe(II)-Glu and Fe(III)-Glu was calculated to be around 8.7×10^{-10} - 2.1×10^{-4} % and 6.1×10^{-2} - 2.4×10^{-1} % using Hyss software at a pH range of 3 - 7, respectively. Cloud water span a wide pH range (3–7), which influences iron speciation and redox cycling. Low pH enhances iron solubility but may reduce Fe–Glu complexation by altering ligand binding. Nevertheless, in polluted regions with elevated iron and amino acid levels, the absolute Fe–Glu concentration may remain appreciable despite a lower complexation fraction. In contrast, marine clouds often contain lower concentrations of both Fe and amino acid (like Glu is around 33 pM collected in Venice on the Sacca San Biagio Island (Barbaro et al., 2011)), leading to a smaller Fe-Glu fraction. Moreover, the concentration of Glu in cloud droplets may increase during the cloud water evaporation,

leading to an increase in the concentration of iron-Glu complexes. This shift could alter atmospheric Fenton reaction dynamics, reducing •OH production, particularly at night (Galloway et al., 2014; Shulman et al., 1997). Similarly, the lower quantum yield of the Fe(III)-Glu under irradiation inhibits the Fe(II)/Fe(III) cycle and •OH generation especially in daytime conditions. Likewise, the variations in light intensity due to diurnal cycles and cloud cover modulate the photolysis rates of iron–ligand complexes and the generation of reactive radicals. Taken together, these factors suggest that the photochemical processes involving Fe–Glu complexes are highly condition-dependent, leading to variable degradation and pathways of amino acids in atmospheric aqueous phases. This underscores the need to incorporate such environmental dependencies into atmospheric models.

In addition, recent studies reported that the average AAs contribution corresponded to 9.1 % of the dissolved organic carbon (DOC) (Bianco et al., 2016), highlighting their significance. Hence, Fe-AAs play a crucial role in iron speciation, stability, and •OH budget in atmospheric aqueous phases, which suggests that the inclusion of Fe-AAs in atmospheric aqueous phase models is essential for accurately estimating •OH production, a key driver of atmospheric oxidation. Moreover, irradiation of Glu in the presence of Fe(III), demonstrated two different mechanisms (•OH mediated and LMCT process) leading to the generation of different products, which can further influence the atmospheric chemical composition, particularly through the formation of aqueous secondary organic aerosols (aqSOA) (Ervens et al., 2014). Overall, the observed generation of NH_4^+ during the Glu photo-degradation suggests a potential transformation pathway from organic nitrogen to inorganic nitrogen species in cloud water, providing a mechanistic link between organic nitrogen and ammonium. This finding is in line with previous reports (Mopper and Zika, 1987) that emphasize the role of amino acids in nitrogen cycling in

the atmosphere. The generation of carboxylic acids further increases atmospheric complexity, as the generated carboxylic acids (e.g., oxalic acid) can complex iron and influence consequent photochemistry. In fact, atmospheric models often simplify the distribution and interactions of transition metal ions (TMIs) with organic compounds, including AAs. This study highlights the crucial role of the LMCT process in AAs oxidation, which should be considered in atmospheric modeling as well.

ACKNOWLEDGMENT

This work was supported by the Agence Nationale de la Recherche of France in the frame of the PRCI project REACTE.

AUTHOR CONTRIBUTION

PC: Investigation, Formal analysis, Writing – original draft**; GM:** Funding acquisition, Review & editing, Supervision**; MS:** Review & editing, Supervision**, GV:** Technical support**; DSF, TS, HH:** Review & editing**; MB:** Conceptualization, Writing-review & editing, Supervision.

REFERENCE

Alpert, P. A., Dou, J., Corral Arroyo, P., Schneider, F., Xto, J., Luo, B., Peter, T., Huthwelker, T., Borca, C. N., Henzler, K. D., Schaefer, T., Herrmann, H., Raabe, J., Watts, B., Krieger, U. K., and Ammann, M.: Photolytic radical persistence due to anoxia in viscous aerosol particles, Nature Communications, 12, 1769, https://doi.org/10.1038/s41467-021-21913-x, 2021.

Angle, K. J., Neal, E. E., and Grassian, V. H.: Enhanced Rates of Transition-Metal-Ion-Catalyzed Oxidation of S(IV) in Aqueous Aerosols: Insights into Sulfate Aerosol Formation in the Atmosphere, Environmental Science & Technology, 55, 10291–10299, https://doi.org/10.1021/acs.est.1c01932, 2021.

Bader, H., Sturzenegger, V., and Hoigné, J.: Photometric method for the determination of low concentrations of hydrogen peroxide by the peroxidase catalyzed oxidation of N,N-diethyl-*p*-phenylenediamine (DPD), Water Research, 22, 1109–1115, https://doi.org/10.1016/0043-1354(88)90005-X, 1988.

Barbaro, E., Zangrando, R., Moret, I., Barbante, C., Cescon, P., and Gambaro, A.: Free amino acids in atmospheric particulate matter of Venice, Italy, Atmospheric Environment, 45, 5050–5057, https://doi.org/10.1016/j.atmosenv.2011.01.068, 2011.

Battaglia Jr., M. A., Weber, R. J., Nenes, A., and Hennigan, C. J.: Effects of water-soluble organic carbon on aerosol pH, Atmospheric Chemistry and Physics, 19, 14607–14620, https://doi.org/10.5194/acp-19-14607-2019, 2019.

Bianco, A., Passananti, M., Perroux, H., Voyard, G., Mouchel-Vallon, C., Chaumerliac, N., Mailhot, G., Deguillaume, L., and Brigante, M.: A better understanding of hydroxyl radical photochemical sources in cloud waters collected at the puy de Dôme station – experimental versus modelled formation rates, Atmospheric Chemistry and Physics, 15, 9191–9202, https://doi.org/10.5194/acp-15-9191-2015, 2015.

Bianco, A., Voyard, G., Deguillaume, L., Mailhot, G., and Brigante, M.: Improving the characterization of dissolved organic carbon in cloud water: Amino acids and their impact on the oxidant capacity, Scientific Reports, 6, 37420, https://doi.org/10.1038/srep37420, 2016.

Bianco, A., Vaïtilingom, M., Bridoux, M., Chaumerliac, N., Pichon, J.-M., Piro, J.-L., and Deguillaume, L.: Trace Metals in Cloud Water Sampled at the Puy De Dôme Station, Atmosphere, 8, 225, https://doi.org/10.3390/atmos8110225, 2017.

Bianco, A., Deguillaume, L., Vaïtilingom, M., Nicol, E., Baray, J.-L., Chaumerliac, N., and Bridoux, M.: Molecular Characterization of Cloud Water Samples Collected at the Puy de

586 Dôme (France) by Fourier Transform Ion Cyclotron Resonance Mass Spectrometry,
587 Environmental Science & Technology, 52, 10275–10285,
588 https://doi.org/10.1021/acs.est.8b01964, 2018.
589 Bianco, A., Passananti, M., Brigante, M., and Mailhot, G.: Photochemistry of the Cloud
590 Aqueous Phase: A Review, Molecules, 25, 423, https://doi.org/10.3390/molecules25020423,
591 2020.
592 Bossmann, S. H., Oliveros, E., Göb, S., Siegwart, S., Dahlen, E. P., Payawan, L., Straub, M.,
593 Wörner, M., and Braun, A. M.: New Evidence against Hydroxyl Radicals as Reactive
594 Intermediates in the Thermal and Photochemically Enhanced Fenton Reactions, The Journal of
595 Physical Chemistry A, 102, 5542–5550, https://doi.org/10.1021/jp980129j, 1998.
596 Buxton, G. V., Greenstock, C. L., Helman, W. P., and Ross, A. B.: Critical Review of rate
597 constants for reactions of hydrated electrons, hydrogen atoms and hydroxyl radicals (·OH/·O−
598 in Aqueous Solution, Journal of Physical and Chemical Reference Data, 17, 513–886,
599 https://doi.org/10.1063/1.555805, 1988.
600 Charbouillot, T., Gorini, S., Voyard, G., Parazols, M., Brigante, M., Deguillaume, L., Delort,
601 A.-M., and Mailhot, G.: Mechanism of carboxylic acid photooxidation in atmospheric aqueous
602 phase: Formation, fate and reactivity, Atmospheric Environment, 56, 1–8,
603 https://doi.org/10.1016/j.atmosenv.2012.03.079, 2012.
604 Christensen, H., Sehested, K., and Corfitzen, H.: Reactions of hydroxyl radicals with hydrogen
605 peroxide at ambient and elevated temperatures, The Journal of Physical Chemistry, 86, 1588–
606 1590, https://doi.org/10.1021/j100206a023, 1982.
607 Deguillaume, L., Charbouillot, T., Joly, M., Vaïtilingom, M., Parazols, M., Marinoni, A.,
608 Amato, P., Delort, A.-M., Vinatier, V., Flossmann, A., Chaumerliac, N., Pichon, J. M., Houdier,

S., Laj, P., Sellegri, K., Colomb, A., Brigante, M., and Mailhot, G.: Classification of clouds sampled at the puy de Dôme (France) based on 10 yr of monitoring of their physicochemical properties, Atmospheric Chemistry and Physics, 14, 1485–1506, https://doi.org/10.5194/acp-14-1485-2014, 2014.

Edwards, K. C., Klodt, A. L., Galeazzo, T., Schervish, M., Wei, J., Fang, T., Donahue, N. M., Aumont, B., Nizkorodov, S. A., and Shiraiwa, M.: Effects of Nitrogen Oxides on the Production of Reactive Oxygen Species and Environmentally Persistent Free Radicals from α-Pinene and Naphthalene Secondary Organic Aerosols, The Journal of Physical Chemistry A, 126, 7361–7372, https://doi.org/10.1021/acs.jpca.2c05532, 2022.

Ervens, B., Sorooshian, A., Lim, Y. B., and Turpin, B. J.: Key parameters controlling OH-initiated formation of secondary organic aerosol in the aqueous phase (aqSOA), Journal of Geophysical Research: Atmospheres, 119, 3997–4016, https://doi.org/10.1002/2013JD021021, 2014.

Gabet, A., Guy, C., Fazli, A., Métivier, H., de Brauer, C., Brigante, M., and Mailhot, G.: The ability of recycled magnetite nanoparticles to degrade carbamazepine in water through photo-Fenton oxidation at neutral pH, Separation and Purification Technology, 317, 123877, https://doi.org/10.1016/j.seppur.2023.123877, 2023.

Galloway, M. M., Powelson, M. H., Sedehi, N., Wood, S. E., Millage, K. D., Kononenko, J. A., Rynaski, A. D., and De Haan, D. O.: Secondary Organic Aerosol Formation during Evaporation of Droplets Containing Atmospheric Aldehydes, Amines, and Ammonium Sulfate, Environmental Science & Technology, 48, 14417–14425, https://doi.org/10.1021/es5044479, 2014.

631 Gligorovski, S., Strekowski, R., Barbati, S., and Vione, D.: Environmental Implications of
632 Hydroxyl Radicals ((•)OH), Chemical Reviews, 115, 13051–13092,
633 https://doi.org/10.1021/cr500310b, 2015.
634 Goldman, M. J., Green, W. H., and Kroll, J. H.: Chemistry of Simple Organic Peroxy Radicals
635 under Atmospheric through Combustion Conditions: Role of Temperature, Pressure, and NOx
636 Level, The Journal of Physical Chemistry A, 125, 10303–10314,
637 https://doi.org/10.1021/acs.jpca.1c07203, 2021.
638 Guo, J., Tilgner, A., Yeung, C., Wang, Z., Louie, P. K. K., Luk, C. W. Y., Xu, Z., Yuan, C.,
639 Gao, Y., Poon, S., Herrmann, H., Lee, S., Lam, K. S., and Wang, T.: Atmospheric Peroxides in
640 a Polluted Subtropical Environment: Seasonal Variation, Sources and Sinks, and Importance of
641 Heterogeneous Processes, Environmental Science & Technology, 48, 1443–1450,
642 https://doi.org/10.1021/es403229x, 2014.
643 Hoops, S., Sahle, S., Gauges, R., Lee, C., Pahle, J., Simus, N., Singhal, M., Xu, L., Mendes, P.,
644 and Kummer, U.: COPASI—a COmplex PAthway SImulator, Bioinformatics, 22, 3067–3074,
645 https://doi.org/10.1093/bioinformatics/btl485, 2006.
646 Kanakidou, M., Myriokefalitakis, S., and Tsigaridis, K.: Aerosols in atmospheric chemistry and
647 biogeochemical cycles of nutrients, Environmental Research Letters, 13, 063004,
648 https://doi.org/10.1088/1748-9326/aabcdb, 2018.
649 Kremer, M. L.: The Fenton Reaction. Dependence of the Rate on pH, The Journal of Physical
650 Chemistry A, 107, 1734–1741, https://doi.org/10.1021/jp020654p, 2003.
651 Long, Y., Charbouillot, T., Brigante, M., Mailhot, G., Delort, A.-M., Chaumerliac, N., and
652 Deguillaume, L.: Evaluation of modeled cloud chemistry mechanism against laboratory

irradiation experiments: The HxOy/iron/carboxylic acid chemical system, Atmospheric Environment, 77, 686–695, https://doi.org/10.1016/j.atmosenv.2013.05.037, 2013.

Mace, K. A., Kubilay, N., and Duce, R. A.: Organic nitrogen in rain and aerosol in the eastern Mediterranean atmosphere: An association with atmospheric dust, Journal of Geophysical Research: Atmospheres, 108, https://doi.org/10.1029/2002JD002997, 2003.

Marion, A., Brigante, M., and Mailhot, G.: A new source of ammonia and carboxylic acids in cloud water: The first evidence of photochemical process involving an iron-amino acid complex, Atmospheric Environment, 195, 179–186, https://doi.org/10.1016/j.atmosenv.2018.09.060, 2018.

Masuda, T., Nakano, S., and Kondo, M.: Rate constants for the reactions of OH radicals with the enzyme proteins as determined by the p-nitrosodimethylaniline method, Journal of Radiation Research, 14, 339–345, https://doi.org/10.1269/jrr.14.339, 1973.

Matos, J. T. V., Duarte, R. M. B. O., and Duarte, A. C.: Challenges in the identification and characterization of free amino acids and proteinaceous compounds in atmospheric aerosols: A critical review, TrAC Trends in Analytical Chemistry, 75, 97–107, https://doi.org/10.1016/j.trac.2015.08.004, 2016.

Mopper, K. and Zika, R. G.: Free amino acids in marine rains: evidence for oxidation and potential role in nitrogen cycling, Nature, 325, 246–249, https://doi.org/10.1038/325246a0, 1987.

Motohashi, N. and Saito, Y.: Competitive Measurement of Rate Constants for Hydroxyl Radical Reactions Using Radiolytic Hydroxylation of Benzoate, Chemical & Pharmaceutical Bulletin, 41, 1842–1845, https://doi.org/10.1248/cpb.41.1842, 1993.

675 Neyens, E. and Baeyens, J.: A review of classic Fenton's peroxidation as an advanced oxidation
676 technique, Journal of Hazardous Materials, 98, 33–50, https://doi.org/10.1016/S0304-
677 3894(02)00282-0, 2003.
678 Penteado, F., Lopes, E. F., Alves, D., Perin, G., Jacob, R. G., and Lenardão, E. J.: α-Keto Acids:
679 Acylating Agents in Organic Synthesis, Chemical Reviews, 119, 7113–7278,
680 https://doi.org/10.1021/acs.chemrev.8b00782, 2019.
681 van Pinxteren, M., Müller, C., Iinuma, Y., Stolle, C., and Herrmann, H.: Chemical
682 Characterization of Dissolved Organic Compounds from Coastal Sea Surface Microlayers
683 (Baltic Sea, Germany), Environmental Science & Technology, 46, 10455–10462,
684 https://doi.org/10.1021/es204492b, 2012.
685 van Pinxteren, M., Zeppenfeld, S., Fomba, K. W., Triesch, N., Frka, S., and Herrmann, H.:
686 Amino acids, carbohydrates, and lipids in the tropical oligotrophic Atlantic Ocean: sea-to-air
687 transfer and atmospheric in situ formation, Atmospheric Chemistry and Physics, 23, 6571–6590,
688 https://doi.org/10.5194/acp-23-6571-2023, 2023.
689 Pye, H. O. T., Nenes, A., Alexander, B., Ault, A. P., Barth, M. C., Clegg, S. L., Collett, J. L.,
690 Fahey, K. M., Hennigan, C. J., Herrmann, H., Kanakidou, M., Kelly, J. T., Ku, I.-T., McNeill,
691 V. F., Riemer, N., Schaefer, T., Shi, G., Tilgner, A., Walker, J. T., Wang, T., Weber, R., Xing,
692 J., Zaveri, R. A., and Zuend, A.: The Acidity of Atmospheric Particles and Clouds, Atmos Chem
693 Phys, 20, 4809–4888, https://doi.org/10.5194/acp-20-4809-2020, 2020.
694 Rachmilovich-Calis, S., Masarwa, A., Meyerstein, N., Meyerstein, D., and van Eldik, R.: New
695 Mechanistic Aspects of the Fenton Reaction, Chemistry – A European Journal, 15, 8303–8309,
696 https://doi.org/10.1002/chem.200802572, 2009.

Renard, P., Brissy, M., Rossi, F., Leremboure, M., Jaber, S., Baray, J.-L., Bianco, A., Delort, A.-M., and Deguillaume, L.: Free amino acid quantification in cloud water at the Puy de Dôme station (France), Atmospheric Chemistry and Physics, 22, 2467–2486, https://doi.org/10.5194/acp-22-2467-2022, 2022.

Samavat, S., Gholami, N., and Nazari, K.: Complexation of Iron (III) With Citrate and Tartarate Anions in Perturbed Aqueous Solutions Using Potentiometry and Difference UV/Vis. and IR Spectrophotometric Methods., Acta Chimica Slovenica, 54, 2007.

Samy, S., Robinson, J., and Hays, M. D.: An advanced LC-MS (Q-TOF) technique for the detection of amino acids in atmospheric aerosols, Analytical and Bioanalytical Chemistry, 401, 3103–3113, https://doi.org/10.1007/s00216-011-5238-2, 2011.

Scheres Firak, D., Schaefer, T., Senff, P., Cheng, P., Sarakha, M., Brigante, M., Mailhot, G., and Herrmann, H.: Fenton-like Reactions in Acidic Environments: New Mechanistic Insights and Implications to Atmospheric Particle-Phase Chemistry, ACS E&ST Air, https://doi.org/10.1021/acsestair.5c00077, 2025.

Shah, V., Jacob, D. J., Moch, J. M., Wang, X., and Zhai, S.: Global modeling of cloud water acidity, precipitation acidity, and acid inputs to ecosystems, Atmospheric Chemistry and Physics, 20, 12223–12245, https://doi.org/10.5194/acp-20-12223-2020, 2020.

Shulman, M. L., Charlson, R. J., and James Davis, E.: The effects of atmospheric organics on aqueous droplet evaporation, Journal of Aerosol Science, 28, 737–752, https://doi.org/10.1016/S0021-8502(96)00469-7, 1997.

von Sonntag, C. and Schuchmann, H.-P.: The Elucidation of Peroxyl Radical Reactions in Aqueous Solution with the Help of Radiation-Chemical Methods, Angewandte Chemie International Edition in English, 30, 1229–1253, https://doi.org/10.1002/anie.199112291, 1991.

720 Soriano-Molina, P., García Sánchez, J. L., Alfano, O. M., Conte, L. O., Malato, S., and Sánchez
721 Pérez, J. A.: Mechanistic modeling of solar photo-Fenton process with Fe^{3+}-EDDS at neutral
722 pH, Applied Catalysis B: Environmental, 233, 234–242,
723 https://doi.org/10.1016/j.apcatb.2018.04.005, 2018.
724 Sorooshian, A., Wang, Z., Coggon, M. M., Jonsson, H. H., and Ervens, B.: Observations of
725 Sharp Oxalate Reductions in Stratocumulus Clouds at Variable Altitudes: Organic Acid and
726 Metal Measurements During the 2011 E-PEACE Campaign, Environmental Science &
727 Technology, 47, 7747–7756, https://doi.org/10.1021/es4012383, 2013.
728 Strathmann, T. J. and Stone, A. T.: Reduction of Oxamyl and Related Pesticides by FeII:
729 Influence of Organic Ligands and Natural Organic Matter, Environmental Science &
730 Technology, 36, 5172–5183, https://doi.org/10.1021/es0205939, 2002.
731 Sun, L., Wu, C.-H., and Faust, B. C.: Photochemical Redox Reactions of Inner-Sphere
732 Copper(II)-Dicarboxylate Complexes: Effects of the Dicarboxylate Ligand Structure on
733 Copper(I) Quantum Yields, The Journal of Physical Chemistry A, 102, 8664–8672,
734 https://doi.org/10.1021/jp982045g, 1998.
735 Tilgner, A., Bräuer, P., Wolke, R., and Herrmann, H.: Modelling multiphase chemistry in
736 deliquescent aerosols and clouds using CAPRAM3.0i, Journal of Atmospheric Chemistry, 70,
737 221–256, https://doi.org/10.1007/s10874-013-9267-4, 2013.
738 Triesch, N., van Pinxteren, M., Salter, M., Stolle, C., Pereira, R., Zieger, P., and Herrmann, H.:
739 Sea Spray Aerosol Chamber Study on Selective Transfer and Enrichment of Free and Combined
740 Amino Acids, ACS Earth and Space Chemistry, 5, 1564–1574,
741 https://doi.org/10.1021/acsearthspacechem.1c00080, 2021.

Vel Leitner, N. K., Berger, P., and Legube, B.: Oxidation of Amino Groups by Hydroxyl Radicals in Relation to the Oxidation Degree of the α-Carbon, Environmental Science & Technology, 36, 3083–3089, https://doi.org/10.1021/es0101173, 2002.

Wang, T. L., Tong, H. W., Yan, X. Y., Sheng, L. Q., Yang, J., and Liu, S. M.: Determination of Volatile Carbonyl Compounds in Cigarette Smoke by LC-DAD, Chromatographia, 62, 631–636, https://doi.org/10.1365/s10337-005-0675-8, 2005.

Wang, Z., Chen, X., Ji, H., Ma, W., Chen, C., and Zhao, J.: Photochemical Cycling of Iron Mediated by Dicarboxylates: Special Effect of Malonate, Environmental Science & Technology, 44, 263–268, https://doi.org/10.1021/es901956x, 2010.

Weller, C., Horn, S., and Herrmann, H.: Photolysis of Fe(III) carboxylato complexes: Fe(II) quantum yields and reaction mechanisms, Journal of Photochemistry and Photobiology A: Chemistry, 268, 24–36, https://doi.org/10.1016/j.jphotochem.2013.06.022, 2013.

Yuan, Y., Feng, L., Xie, N., Zhang, L., and Gong, J.: Rapid photochemical decomposition of perfluorooctanoic acid mediated by a comprehensive effect of nitrogen dioxide radicals and Fe^{3+}/Fe^{2+} redox cycle, Journal of Hazardous Materials, 388, 121730, https://doi.org/10.1016/j.jhazmat.2019.121730, 2020.